*aerospace*

MDPI

*Article*

# A Novel Composite Helicopter Tail Rotor Blade with Enhanced Mechanical Properties

**Anton Hadăr [1,2,3], Andrei-Daniel Voicu [1], Florin Baciu [1], Daniel Vlăsceanu [1], Daniela-Ioana Tudose [1] and Ştefan-Dan Pastramă [1,*]**

[1] Department of Strength of Materials, Faculty of Industrial Engineering and Robotics, University Politehnica of Bucharest, 313 Splaiul Independenței, Sector 6, 060042 Bucharest, Romania; anton.hadar@upb.ro (A.H.); voicu_andrei2001@yahoo.com (A.-D.V.); florin.baciu@upb.ro (F.B.); daniel.vlasceanu@upb.ro (D.V.); daniela.tudor@upb.ro (D.-I.T.)
[2] Academy of Romanian Scientists, 3 Ilfov Street, Sector 5, 050045 Bucharest, Romania
[3] Technical Sciences Academy of Romania, 26 Dacia Boulevard, Sector 1, 030167 Bucharest, Romania
* Correspondence: stefan.pastrama@upb.ro; Tel.: +40-72-2225212

**Abstract:** This paper describes the transition towards a composite structure, with the same overall aerodynamic characteristics, for a tail rotor blade of an IAR330 helicopter. The newly proposed structure of the composite blade is made of a carbon-roving spar embedded with epoxy resin, a hexagonal-cell honeycomb core manufactured by fused deposition modelling, and an outer skin made of multiple carbon-fibre-reinforced laminae. The blade was manufactured by the authors using the hand lay-up method at a scale of 1:3 with respect to the real one, and all stages of the manufacturing process are extensively described in the paper. The experimental tests were performed on an Instron 8872 testing machine by applying a bending force on its free edge, similar to the testing methodology employed by various composite blade manufacturers. A three-dimensional numerical model of the tail rotor blade was conceived, analysed using the finite element method, and validated by comparing the numerical and experimental values of the maximum bending force. Further, the model was used for a complex finite element analysis that showed the very good behaviour of the proposed composite blade during flight and emphasized the main advantages brought by the proposed composite structure.

**Keywords:** helicopter composite blade; finite element analysis; hand lay-up manufacturing; fused deposition modelling; fluid flow analysis



**Citation:** Hadăr, A.; Voicu, A.-D.; Baciu, F.; Vlăsceanu, D.; Tudose, D.-I.; Pastramă, Ş.-D. A Novel Composite Helicopter Tail Rotor Blade with Enhanced Mechanical Properties. *Aerospace* **2023**, *10*, 647. https://doi.org/10.3390/aerospace10070647

Academic Editor: Kyungil Kong

Received: 5 June 2023
Revised: 17 July 2023
Accepted: 17 July 2023
Published: 19 July 2023



## 1. Introduction

Composite materials undoubtedly represent the future of aircraft manufacturing. This tendency has increased over the past decade, with modern aircraft containing high percentages of fibre-reinforced plastics and lightweight cores coming out of the production lines. Although the benefits are clearly visible, the high cost of transition to a modern aircraft can be diminished by replacing certain metallic components of aeroplanes or helicopters of older generations with composite ones, thus enhancing the overall performance and increasing the lifetime of the whole structure.

The main advantages of composites, as opposed to metallic components, include the following: a high strength-to-weight ratio (the mass density of carbon fibre is about 24% of one of steel and about 70% of an aluminium one) [1], proven durability expressed by reduced maintenance costs and long-term stability [2], new design possibilities (a composite component can replace an entire metal assembly) [3], and ease of manufacturing, thanks to recent advantages in the field of digital composite manufacturing [4].

The most common composite materials used in the aeronautical industry include carbon-fibre-, glass-fibre-, and aramid-fibre-reinforced epoxy, which can be tailored to obtain the desired mechanical characteristics [5]. The most used matrix for a composite

material is high-performance epoxy resin, but there are also other alternatives that can be employed, such as phenolics, polyesters, or polyimides [6]. Both thermoplastic and thermosetting polymers can be used, depending on the application. For the inner core of lightweight structures, such as the blades or wings, the main structures used are foams (polyurethane, polypropylene, or polyvinyl chloride) or honeycombs/lattice structures, which facilitate custom mass distribution across the structure [7].

The aircraft worth mentioning that contain a high amount of composite materials are the Boeing 787 Dreamliner and the Airbus 350 (approximately 50%) [8], Solar Impulse (83% of the structure) [9], Lockheed Martin F-35 Lightning II (nearly 35%) [10], and Lockheed Martin F-22 Raptor (25%) [11].

In the case of helicopters, the main rotor and the tail rotor are systems manufactured partially or entirely from specially designed composites [12]. The overall structure of the blade consists of a spar, a lightweight honeycomb core, and the thin outer skin of the blade. These represent the main three components that can be found on most composite rotor blades, some of which are mentioned in Figure 1.

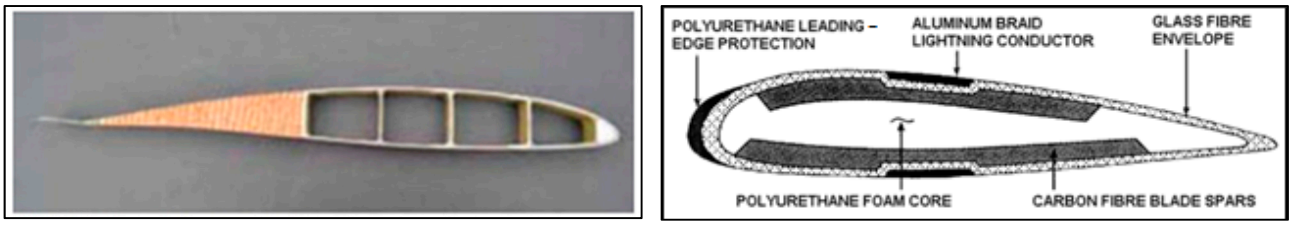


(**a**) (**b**)

**Figure 1.** Examples of composite blades with similar inner structures. (**a**) AH-64 Apache rotor blade section [13]. (**b**) Dowty rotor composite propeller blade section [14].

The mechanical response of different types of helicopter blades and the possibility of replacement of the metal components with composite materials in their construction is currently the subject of extensive scientific research, with both numerical analyses and experimental tests being undertaken in recent years.

The implementation of advanced composite technology for a rotor blade of an unmanned ILX-27 helicopter was described in [15]. The paper presents all stages of the design of the blade structure in parallel with composite technology development (basic technologies, processes, equipment, and cost), with all data being gathered and documented during the execution of the proposed project. Rasuo [16,17] presented the fabrication process and analysis of the mechanical behaviour of a tail rotor blade made of a laminated composite and mounted on a heavy transport helicopter. Different mechanical tests were undertaken: static tests, involving an experimental evaluation of torsional and flexional blade stiffness and its elastic axis position; dynamic tests of vibratory characteristics (natural frequency, vibration modes, and damping ratio); and fatigue testing of the blade to detect laminate separation, tolerance, and distortion of cross sections of the structure. A comprehensive experimental campaign conducted on the main and tail rotor composite material blades of a medium-sized helicopter was described by Luczak et al. [18]. The rear helicopter rotor blade was made of a sandwich composite covered with an aluminium sheet, while the blades from the main rotor were manufactured from glass-fibre-reinforced plastics. In the blade structures, the spar was reinforced with glass-roving material, and the honeycomb elements were made from Nomex or glass epoxy. The study included static tests made on the tail rotor blade with the application of electrical and fibre-optic strain gauges, dynamic strain measurements on the tail rotor blade, and experimental modal analyses using piezoceramic accelerometers, microflow, and laser vibrometer sensors. The strength calculation of a prototype of the main rotor blade spar used in an unmanned helicopter was performed by Kliza et al. [19] using the finite element method. Eight-layer-laminated composites with $[0/45/-45/90]_S$ and $[(0/90)_4]_T$ laminae distributions were considered as the material for

the spar, both with carbon or glass fibre reinforcements. Finite element analyses (FEAs) were performed to find the stress distribution due to gravitational, lift, and centrifugal forces and the moment of torsion. Conclusions were drawn regarding the best laminate arrangement for the studied structure. Similar finite element calculations were undertaken in [20] for a blade from the tail rotor of a Eurocopter EC225 Super Puma helicopter. The authors compared two variants of the blade, one made of aluminium and the other made of different composite materials like glass fabric/epoxy, carbon/epoxy, and kevlar149, and showed that carbon/epoxy with [0/90] and [−45/45] orientation has better strength than aluminium, being able to sustain higher loads. The strength analysis of composite tail rotor blades of a helicopter HT-40, tested under static and fatigue load spectra, is presented by Maksimovic et al. [21]. The authors used two models to obtain the aerodynamic loads of helicopter tail rotor blades: an isolated tail rotor blade and a complete helicopter, modelled including the fuselage together with main and tail rotor blades. The mechanical response of helicopter blades made of composite materials was also investigated in [22]. The authors studied the stress field, free vibration, and time response on different configurations and used a straight metallic rotating structure and a swept-tip blade made of an orthotropic material for verification and validation purposes. Further, a straight and a double-swept blade with a realistic airfoil were studied.

Other studies on composite helicopter blades have focused on the analysis of cracks initiated in the areas near the interface between the foam core and the adhesive [23]; the study of the deformation of a rotor blade made of polymer composite materials with active geometry control using embedded piezoelectric actuators [24]; the investigation of possible defects in the composite structure of helicopter rotor blades using combined neutron and X-ray radiography [25]; numerical analyses to simulate the response of composite rotor blades under high-velocity impact loads due to bird strikes [26,27]; the optimum structural design of composite helicopter blades using a genetic-algorithm-based optimizer [28]; computational fluid dynamics simulations of the Hover Validation and Acoustic Baseline, Smart Twisting Active Rotor, and Active Twist Rotor blades in hover [29]; the free-vibration behaviour of multi-layer composite beams reinforced with graphene platelets resting on a viscoelastic foundation [30]; etc.

In this paper, the authors develop a new composite tail rotor blade to replace the currently used aluminium one for an IAR330 helicopter of the Romanian Air Forces, a license-built version of the Aérospatiale SA 330 Puma helicopter. The proposed new structure is made of a carbon-roving spar embedded with epoxy resin, a hexagonal-cell honeycomb core manufactured by fused deposition modelling, and an outer skin made by hand lay-up of multiple carbon-fibre-reinforced laminae. A numerical model of the composite tail rotor blade is developed at a scale of 1:3 using tensile, bending, and compression mechanical properties previously obtained in several mechanical tests [31,32]. The model is validated using experimental measurements made on a blade manufactured by the authors. Finally, more complex numerical analyses using the validated model are presented, using as input data the results of a computational fluid dynamics (CFD) analysis previously undertaken by the authors [33].

## 2. Description of the Studied Blade

The currently used aluminium tail rotor blade of an IAR330 helicopter has a length of 1244.3 mm, being characterized by an NACA0012 symmetric airfoil and no blade twist along the length of the blade. The chord measures 186.5 mm, and the total mass is approximately 2.68 kg. A model of the aluminium blade during aerodynamic analysis inside a subsonic wind tunnel is presented in Figure 2 [33].

The components of the current version of the tail rotor blade are manufactured from three aluminium alloys with different physical and mechanical properties, capable of withstanding in-flight loads. The shape of the newly proposed blade has not been the subject of any adaptation since it is designed to equip the same helicopter as the metal blade, with the enhanced performances being only the result of material upgrades.

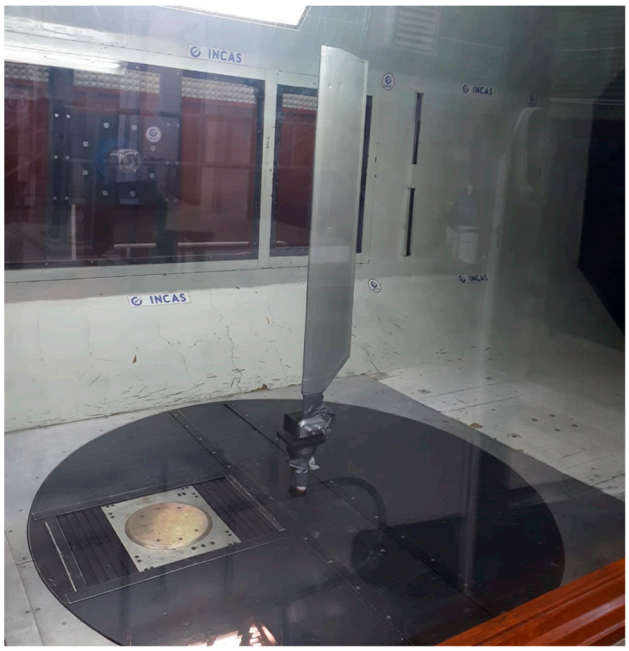


**Figure 2.** IAR330 tail rotor blade model [33].

The materials chosen for the composite upgrade of the tail rotor blade were determined after broad research regarding composite blade manufacturing to produce a balanced structure. Their main characteristics are presented below:

- The skin of the blade is made of a carbon-fibre-reinforced polymer, with Derakane Momentum 470–300 epoxy resin utilized for the composite matrix and a twill 2/2 carbon fibre weave [0/90], model GG285T, used for reinforcing the composite. The epoxy resin is characterized by very good mechanical properties, high resistance to chemicals, and great malleability. The carbon fibre weave disposes of 3000 fibres per filament and a linear density of 200 tex.
- The spar of the blade, as the element that offers greater strength to the structure, is made of T300 carbon fibres (roving), oriented in accordance with the length of the blade. These fibres are recognized for their outstanding performance, quality, and consistency in processing and have been used in aerospace applications over the past 30 years, thus being adequate for this structure. The carbon fibre roving is embedded with the same epoxy resin as the skin in order to produce a high-strength unitary component.
- The honeycomb core of the blade is manufactured from a thermoplastic-extruded chlorinated polyethylene filament, model CPE CF112 Carbon. The filament exhibits satisfactory mechanical properties because it contains milled carbon microfibres. This model also offers a good quality–price ratio for the designated purpose, being adequate for fatigue testing.

In Table 1, the properties of the above-mentioned materials are listed, as offered by the manufacturer's data sheets.

Table 2 contains the mechanical properties which were previously determined from tensile and compression tests, carried out in the Strength of Materials Laboratory from the University Politehnica of Bucharest [31,32].

**Table 1.** Properties of the materials used for the composite blade.

| Material | Property Type | Value |
|---|---|---|
| GG 285T twill weave 2/2 [34] | Fabric type | Twill 2/2 |
| | Ply thickness | 0.28 mm ± 2.5% |
| | Distribution | 600 g of filament |
| | Fibre type | High-resistance carbon fibre 3k—200 tex |
| | Thread count | 7.0 ends/cm |
| | Weight distribution | 142 g/m$^2$ (50% warp, 50% weft) |
| | Density | 1.79 g/cm$^3$ |
| Derakane Momentum 470–300 epoxy resin [35] | Dynamic viscosity | 325 mPa·s |
| | Kinematic viscosity | 300 cSt |
| | Density | 1.17 g/cm$^3$ |
| | Heat distortion temperature | 150 °C |
| | Glass transition temperature | 165 °C |
| T300 carbon fibre roving [36] | Density | 1.76 g/cm$^3$ |
| | Filament diameter | 7 µm |
| | 3K linear roving density | 198 g/1000 m |
| | Coefficient of thermal expansion | 0.41 × 10$^{-6}$/°C |
| | Specific heat | 0.19 Cal/g·C |
| | Thermal conductivity | 0.025 Cal/cm·s·°C |
| | Electric resistivity | 1.7 × 10$^{-3}$ Ω·cm |
| | Chemical composition | 93% carbon<br>Na + K < 50 ppm |
| CPE CF112 Carbon filament embedded with milled carbon microfibres [37] | Density | 1.16 g/cm$^3$ |
| | Diameter tolerance | ±0.10 mm |
| | Weight | 600 g filament (+250 g roll) |
| | Printing temperature | 250–270 °C |
| | Hot pad | 70–85 °C |
| | Bed adhesive | Magigoo, 3Dlac |
| | Part cooling fan | 0–15% |
| | Printing speed | 20–40 mm/s |

The tensile properties of each material were determined in accordance with the ASTM D3039 standard for composite tensile testing [38] using an Instron 8872 servo-hydraulic testing system, with a load cell of 100 kN. The tensile properties of the 3D-printed material were determined on dog-bone-shaped specimens printed in three different directions (flatwise, sidewise, and lengthwise) to assess the orthotropic behaviour of the material and to select the best manufacturing direction for the honeycomb core. The results were obtained using the Dantec Q400 Standard digital image correlation system. The compression properties were determined on the same Instron system, equipped with specific adapters, and in compliance with the ASTM C365 standard for compression testing of core materials [39].

The tensile and compression properties obtained during mechanical testing revealed a higher strength than one of aluminium [40], making them more suitable for the cyclic loading characteristic specific to all aircraft structures. Greater mechanical performances mean greater reliability in service conditions, contributing to increasing flight safety conditions.

**Table 2.** Mechanical properties determined for the materials used for the composite blade [31,32].

| Blade Component Material | Property Type | Mechanical Property |
|---|---|---|
| Skin—carbon-fibre-reinforced polymer (3K GG 285 T carbon fibre weave embedded with Derakane Momentum 470–300 epoxy resin) | Tensile properties | Young's modulus—41,733.38 MPa<br>Yield Strength—448.58 MPa<br>Tensile strength—480.57 MPa<br>Percent elongation at break—1.429%<br>Poisson's ratio—0.353 |
| Spar—carbon-fibre-reinforced polymer (T300 carbon fibre roving embedded with Derakane Momentum 470–300 epoxy resin) | Tensile properties | Young's modulus—65,839.65 MPa<br>Yield strength—385.17 MPa<br>Tensile strength—587.77 MPa<br>Percent elongation at break—1.037%<br>Poisson's ratio—0.35 |
| Honeycomb core with hexagonal cells—CPE CF112 Carbon filament embedded with milled carbon microfibres | Tensile properties (Printed flatwise) | Young's modulus—4448.10 MPa<br>Yield strength—40.26 MPa<br>Tensile strength—47.29 MPa<br>Percent elongation at break—1.85%<br>Poisson's ratio—0.388 |
| | Tensile properties (Printed sidewise) | Young's modulus—4783.22 MPa<br>Yield strength—38.86 MPa<br>Tensile strength—44.97 MPa<br>Percent elongation at break—1.64%<br>Poisson's ratio—0.316 |
| | Tensile properties (Printed lengthwise) | Young's modulus—3175.97 MPa<br>Yield strength—29.56 MPa<br>Tensile strength—31.50 MPa<br>Percent elongation at break—1.38%<br>Poisson's ratio—0.225 |
| | Compression properties | Compression modulus—3184.90 MPa<br>Yield strength in compression—29.48 MPa<br>Ultimate strength in compression—31.40 MPa<br>Percent shortening at break—1.38% |

## 3. Manufacturing and Testing of the New Blade

### *3.1. The Manufacturing Process*

The composite version of the tail rotor blade was manufactured at a scale of 1:3 from the previously presented materials by maintaining the same inner dimensions of the components. The hand lay-up method chosen for this task represents the most widespread manufacturing method, although it is mostly dependent on the practical experience of the manufacturer. The main stages in the manufacturing process are as follows:

- Manufacturing a two-part mould;
- Manufacturing a temporary model of the blade, which is necessary for adjusting the composite blade inside the mould;
- Manufacturing the skin of the blade inside each of the two moulds;
- Positioning the semi-honeycomb core in each of the two moulds;
- Manufacturing the spar of the blade, positioned in the leading-edge area;
- uniting the two moulds and locking them in place;
- Extracting the composite blade from the moulds and applying surface finishing operations.

The manufacturing process began by modelling a provisory blade from a malleable commercial resin, shaped in accordance with the NACA0012 aerodynamic profile. The foot of the blade was later added to the aerodynamic section (the final shape is presented in Figure 3), alongside the two aluminium moulds. This blade was then divided into three parts corresponding to the dimensions of each component of the tail rotor blade. The parts were used to adjust the components inside the moulds, thus ensuring that the dimensions were respected and a proper adhesion between the components was achieved.

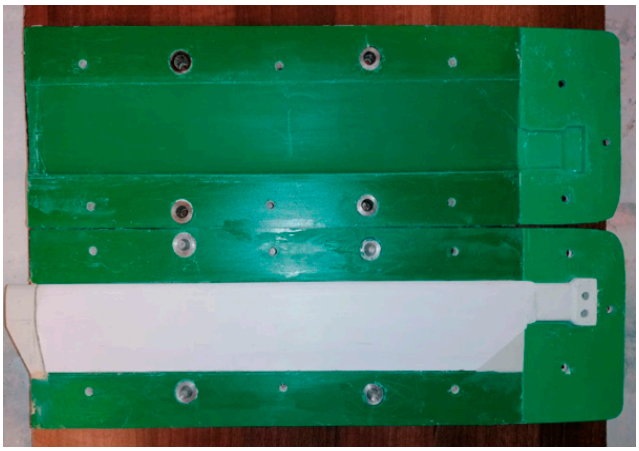

**Figure 3.** The two moulds and the provisory blade used for adjusting the composite blade.

The honeycomb core of the blade was realized using fused deposition modelling (FDM) on a custom 3D Xcub printer from two horizontally symmetric components, which were united at the middle plane, when the two moulds were locked in position. The printing equipment is characterized by an optimum printing speed of 50 mm/s and a maximum printing volume of (42 × 42 × 47) cm. The honeycomb components were printed at a resolution of 0.1 mm, with a total manufacturing time of approximately 8 h. The printing pad of the equipment was heated at a temperature of 30 °C in order to help preserve the shape of the component, as well as to facilitate detachment.

The honeycomb core components and the equipment used for manufacturing can be seen in Figure 4.

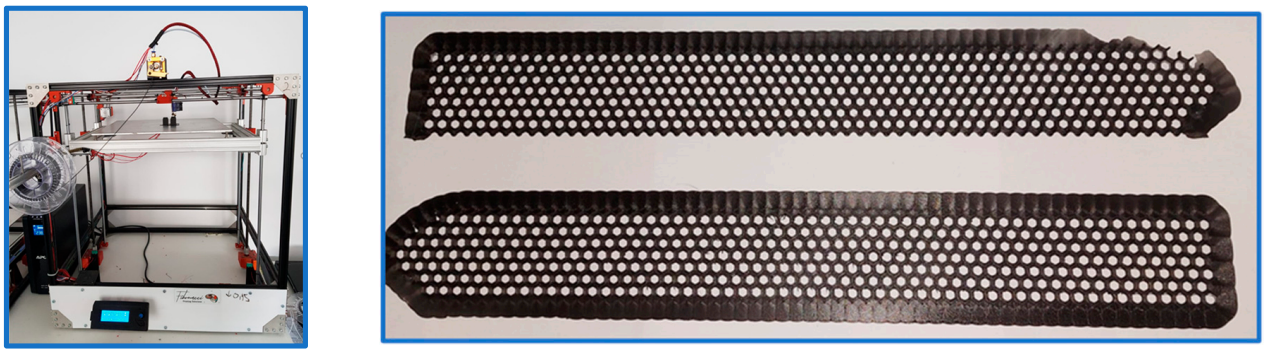

(**a**) (**b**)

**Figure 4.** The honeycomb core of the tail rotor blade: (**a**) 3D printer used for manufacturing the honeycomb, (**b**) the two symmetric honeycomb components.

The first component to be placed inside the moulds was the skin. Before the first material layer was placed, a mould-release chemical agent was applied on the inner sides of the moulds. Three layers of GG285T carbon fibre twill weave were placed in the moulds and bonded together with the Derakane Momentum 470–300 to construct the skin of the tail rotor blade, adjusted to the NACA0012 profile shape. After the epoxy resin was cured for approximately 24 h, any material surplus was adjusted at the middle plane level. The orientation of the fibres was kept the same for the entire skin of the blade, with a 0° orientation corresponding to the fibres positioned on the length of the blade and a 90° orientation corresponding to the fibres parallel to the blade chord line.

Afterwards, the honeycomb core was placed on the skin of the blade and its position was adjusted with the aid of additional components, as shown in Figure 5.

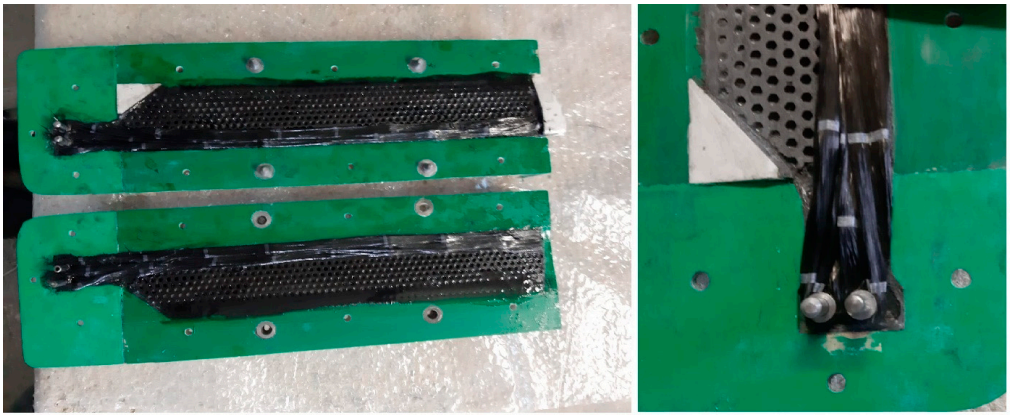

**Figure 5.** Placing the components inside the moulds.

The T300 carbon roving consists of unitary unidirectional fibres positioned lengthwise, adjusted to fit the dimensions of the tail rotor blade spar. The fibres were positioned around two metal bushings, which represent the mounting points of the tail rotor blade to the antitorque rotor. These fibres have the best tensile properties of all the materials of the composite blade. The spar was obtained by applying the same epoxy resin on the fibres, thus uniting them in a single solid body. The wooden frame, which was conceived to lock the two moulds in place with screws placed on all sides, is depicted in Figure 6, as well as the composite tail rotor blade after applying the surface finish.

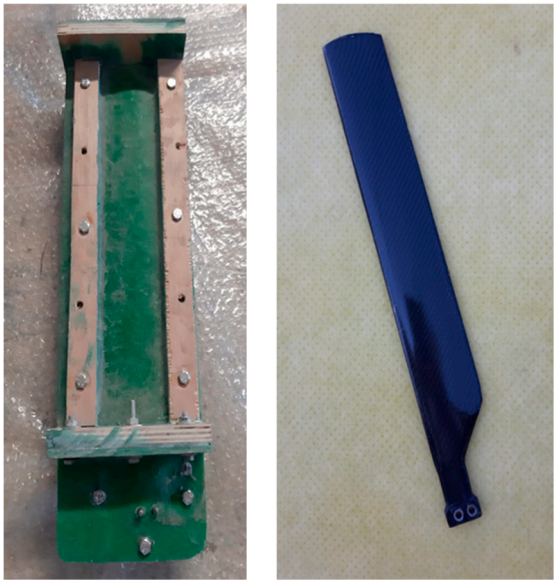

(**a**) (**b**)

**Figure 6.** Final stages of the manufacturing process: (**a**) the manufacturing moulds locked into place, (**b**) final composite blade after surface finish was applied.

The curing process took place at room temperature (approximately 23 °C) in relatively low humidity for a period of at least 24 h. After the blade was removed from the moulds, the following finishing operations were applied: the removal of excess surfaces, cleaning of the mould-release chemical agent, and applying a protective varnish.

### *3.2. Experimental Setup and Testing*

The experimental procedure consisted of applying a bending force on the free edge of the composite tail rotor blade, while the other edge was fixed on a metal support.

The testing procedure is similar to the one used by composite blade manufacturers to assess fatigue strength [41–43]. An Instron 8872 testing machine with a 25 kN load cell was used to apply a specific load on the free edge of the blade. The metal support beam was chosen rigid enough in order to prevent the entire assembly from bending at the moment the force was applied. The blade was fastened to the beam with two bolts at the foot of the blade, as shown in Figure 7.

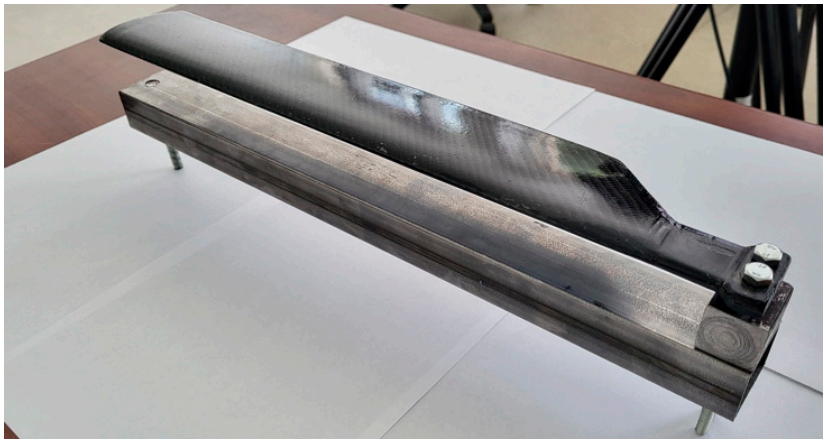

**Figure 7.** The composite blade fixed on the rigid metal support.

The entire beam–blade assembly was positioned in the testing machine, and the force was applied to the tip of the composite tail rotor blade (Figure 8).

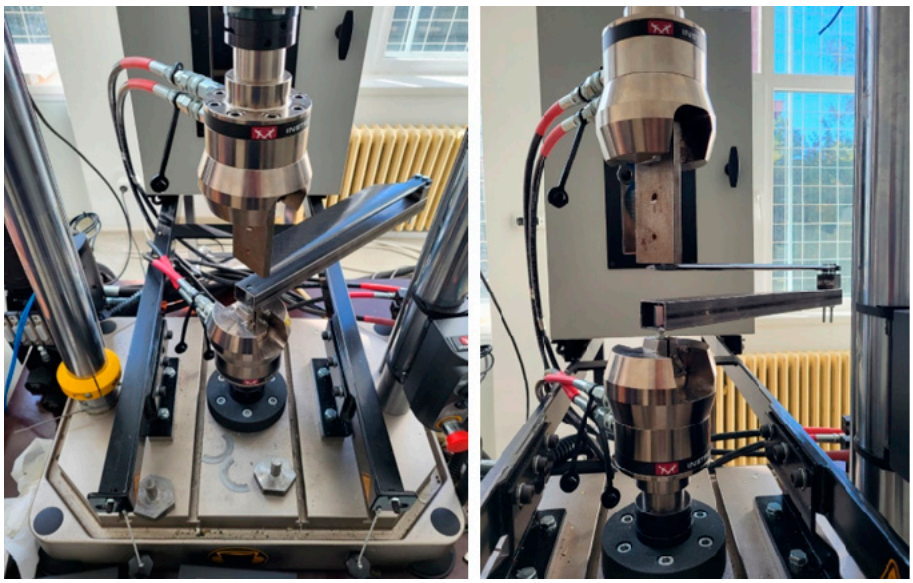

**Figure 8.** The experimental set-up.

A total of five individual tests were realized with a constant displacement of 2 mm/min and a maximum displacement of 10 mm, adjusted using the dedicated software, WaveMatrix, of the testing machine. The reaction force was measured by using the testing system and returned in tabular form. Ambient conditions consisted of low UV exposure, under 60% air humidity, and an ambient temperature of 23 °C. The force–displacement curves obtained for the experimental tests are presented in Figure 9 and Table 3.

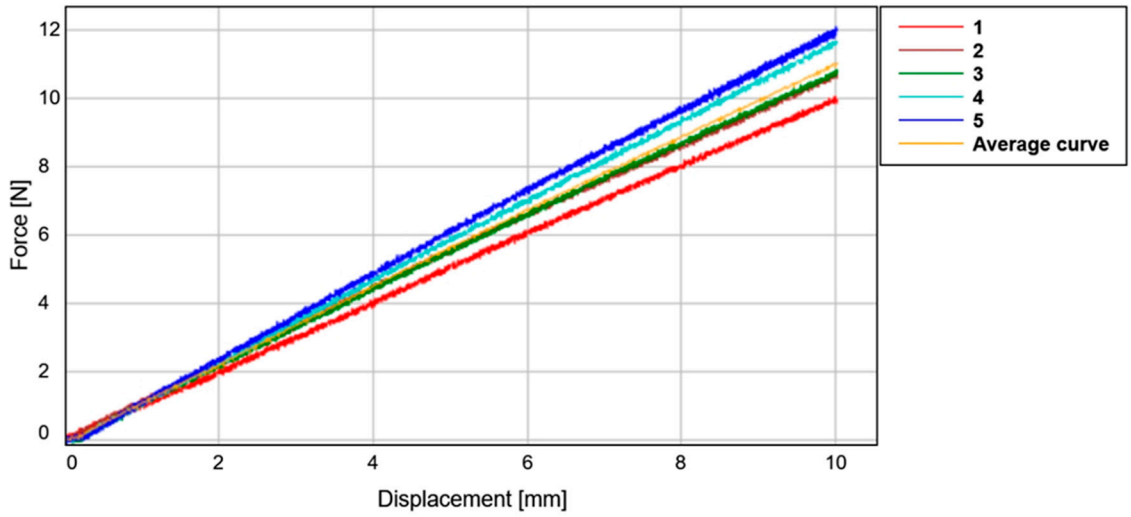


**Figure 9.** Force–displacement curve for the composite blade test.

**Table 3.** Main results of the tail rotor blade tests.

| Test Number | Maximum Force (N) | Displacement (mm) | Time (s) |
|---|---|---|---|
| Test-1 | 10.049 | 10 | 300.77 |
| Test-2 | 10.729 | 10 | 300.66 |
| Test-3 | 10.852 | 10 | 300.85 |
| Test-4 | 11.714 | 10 | 300.76 |
| Test-5 | 12.092 | 10 | 300.45 |
| Average | 11.087 | 10 | 300.70 |

The maximum forces for the five experimental tests were between 10.049 and 12.092 N, with an average value of 11.087 N. During the test, no plastic deformation was observed, and the blade returned to its original position.

## 4. The Finite Element Model

The three-dimensional finite element model of the blade was conceived in Ansys Workbench [44], at the same scale of 1:3 with respect to the real dimensions. The 3D mesh consisted of 20-node solid elements (Solid 186) for the honeycomb core and 10-node tetrahedral elements (Solid 187) for the blade spar and skin, with a selected element size of 2 mm. The entire model comprises 5,057,655 nodes and 2,240,226 elements, which resulted in a significant processing time of almost two days. More than half of these elements were placed on the honeycomb due to its irregular shape.

The geometrical model of the tail rotor blade is presented in Figure 10. The material properties for each component of the composite blade considered for the FEA are those listed in Tables 1 and 2. The skin of the blade was defined with the Ansys Composite PrepPost (ACP Pre) module of the Ansys program in order to define the properties of the warp and the weft, as well as the fabric orientation, which was maintained the same across the entire lay-up [0/90].

The boundary conditions employed in the FEA consisted of the fixed support command, applied vertically, on the inner surfaces of the tail rotor spar, while a displacement of 10 mm was imposed on the free edge of the tail rotor blade, as illustrated in Figure 11.

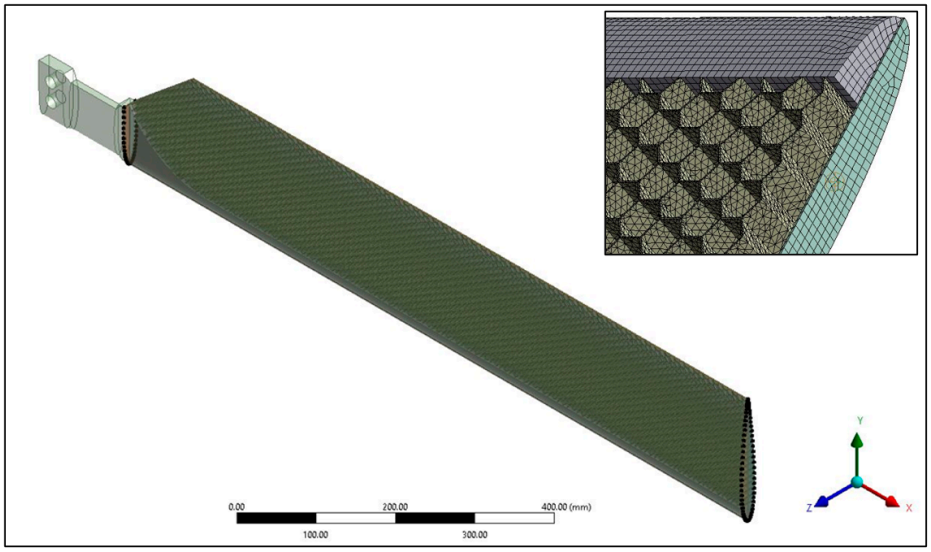


**Figure 10.** The geometrical model of the tail rotor blade.

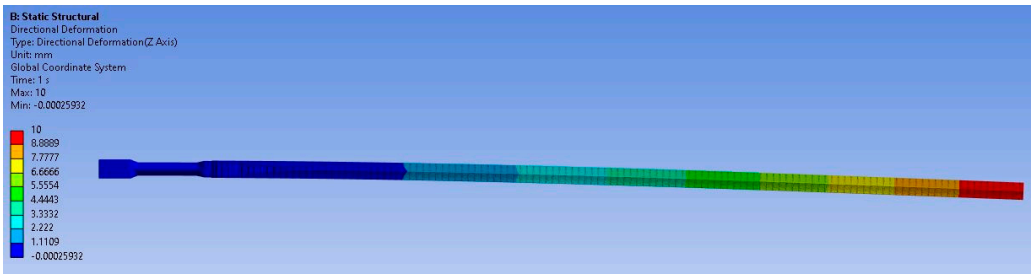


**Figure 11.** Displacement applied on the free edge of the blade.

The main results obtained from the FEA are presented in Figures 12–16. The maximum total displacement of the blade is, as expected for a bending load, on the free edge of the blade and manifested only in the vertical plane in which the displacement is orientated. The maximum equivalent elastic strain of 0.4695% occurs in very small, localized areas on the honeycomb core, in the cell joints of the hexagonal cells, due to the irregular shape, which produces stress concentration effects. Much smaller values can be noticed on the other components, as can be seen in Figure 13.

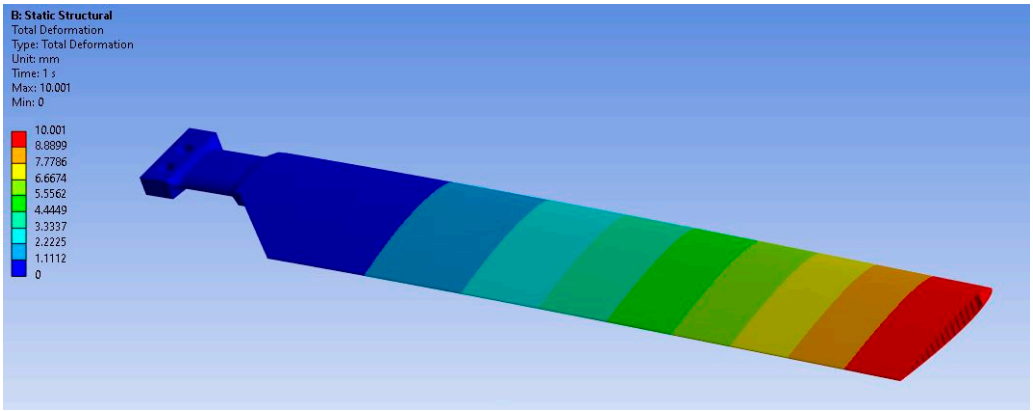


**Figure 12.** Total displacements of the composite tail rotor blade.

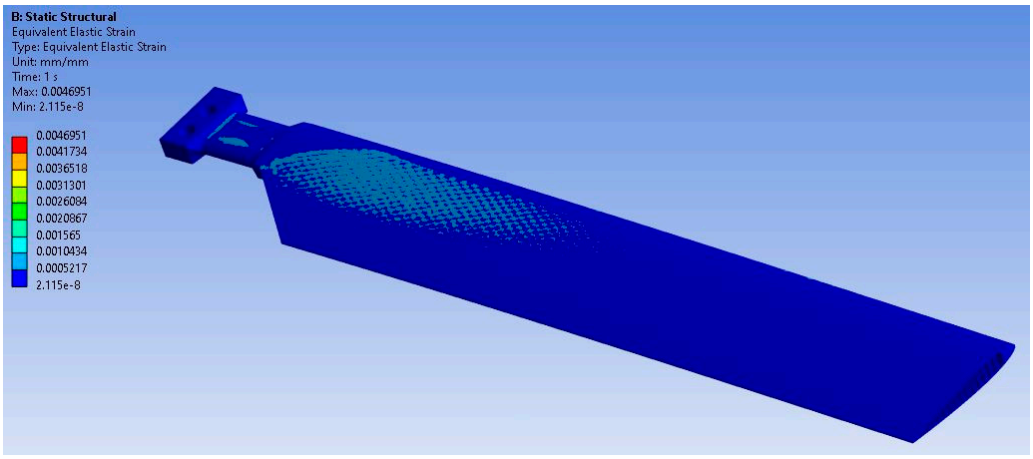


**Figure 13.** Equivalent elastic strain of the composite tail rotor blade.

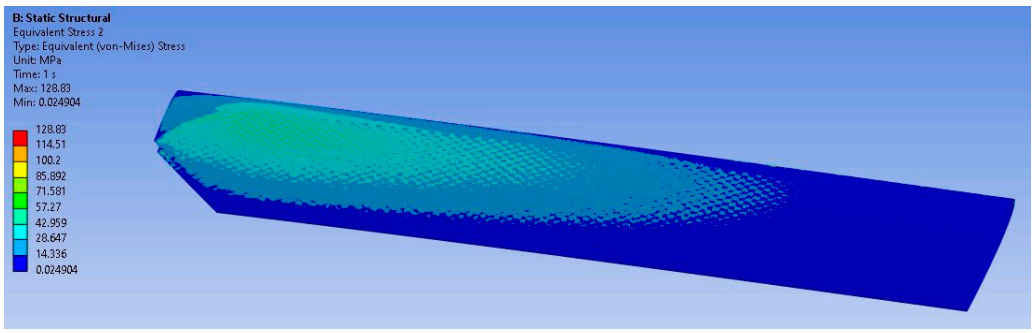


**Figure 14.** Von Mises equivalent stress distribution on the skin of the composite blade.

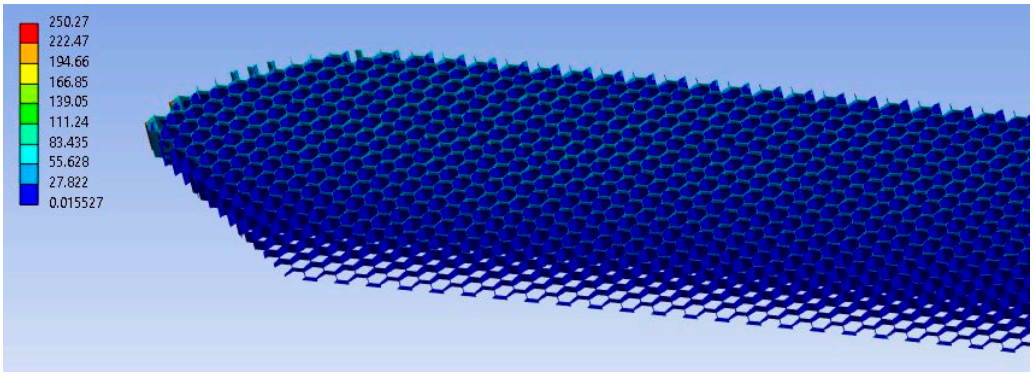


**Figure 15.** Equivalent stress distribution on the honeycomb hexagonal cells.

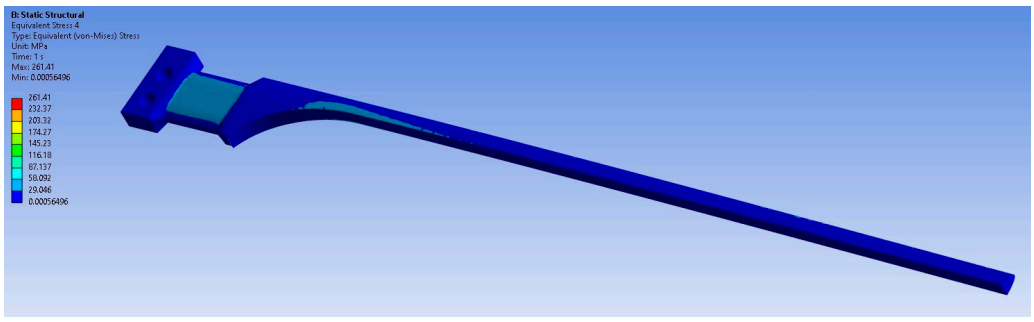


**Figure 16.** Von Mises equivalent stress distribution on the spar of the tail rotor blade.

In Figure 14, it can be seen that the maximum value of the equivalent von Mises stress is 128.83 MPa. This value occurs in the carbon-fibre-laminated skin of the blade, located

towards the middle section of the blade. The honeycomb core exhibits a maximum stress of 250.27 MPa (Figure 15) but in a very small area located both on the upper side and on the lower side. Because this is an extremely localized effect, it does not produce the failure of the core. In what concerns the spar element, the maximum stress of 261.41 MPa is localized on the foot of the blade; this is the reason why this element is manufactured to ensure a high degree of stiffness (Figure 16).

From the FEA, the reaction at the point where the externally applied bending force is located can be obtained and has a value of 10.405 N. This value will be further used to validate the proposed finite element model by comparison with the one measured experimentally, as shown in the next paragraph.

## 5. Discussion of the Results

In Table 4, a comparison between the numerical and experimental values of the maximum force is listed. The difference between the two results is small, thus validating the numerical model. One can conclude that the numerical model reproduces the mechanical behaviour of the real composite blade with very good accuracy.

**Table 4.** Experimental vs. numerical results.

| Tail Rotor Blade | Maximum Force (N) |
|---|---|
| Composite tail rotor blade (mean value) | 11.087 |
| FEA of composite tail rotor blade | 10.405 |
| Error (%) | 6.15 |

Following the experimental validation, the proposed numerical model may be utilized for more complex studies to simulate the mechanical behaviour of the tail rotor blade under typical flight procedures. Also, the proposed experimental setup can be further used for the fatigue testing of the blade by repeating the test for any number of cycles.

Another conclusion that can be drawn comes from the analysis of the results shown in Table 5, where a comparison is made between the mass of the newly proposed blade and the one made of aluminium that is currently in use on an IAR330 helicopter. A significant mass reduction can be obtained by manufacturing the tail rotor blade with composite materials. The overall estimated decrease in the mass is 41.54%. The mass reduction for each of the blade components is also listed in Table 5.

**Table 5.** Mass comparison (metal blade vs. composite blade).

| Blade Component | Percentage of the Total Blade Volume | Metal Blade (kg) | Composite Blade (kg) | Mass Reduction (%) |
|---|---|---|---|---|
| Spar | 21.03% | 1.6075 | 1.0478 | 34.82 |
| Honeycomb core | 20.32% | 0.5724 | 0.2478 | 56.71 |
| Skin | 58.65% | 0.5583 | 0.3052 | 45.33 |
| Total | 100% | 2.7383 | 1.6008 | 41.54 |

It should also be underlined that the presented methodology has some limitations: i. blade testing can only be realized for small loads; ii. the testing procedure can only be regarded as a single cycle from a fatigue testing procedure, and therefore, the best way to evaluate the fatigue strength of the blade is to repeat the previously presented test for a high number of cycles; and iii. the position of the load on the blade edge is approximated as to reproduce the load placement position from the finite element analyses.

## 6. Complex FEA: Aerodynamic Loading of the Tail Rotor Blade

The validated numerical model is now used to verify the overall performances of the tail rotor blade in a complex numerical analysis, in which the new proposed blade is loaded

with the aerodynamic pressures previously obtained from a fluid flow analysis realized in Fluent, at an airflow speed of 50 m/s, and with the blade fixed in a vertical position. The value of the airflow speed was selected due to the fact that the pressures obtained from the CFD analysis were validated by using a real-scale model of the blade positioned inside a subsonic wind tunnel [33].

During helicopter flight, the blade incidence can vary in a range between +2.5° and −15.5°, depending on the manoeuvers the pilot is attempting. The four main blade incidences selected for the FEA are the following:

- $\alpha = +2.5°$—represents the maximum positive incidence that the tail rotor blade can have, at any flight regime, operated by the helicopter pilot;
- $\alpha = 0°$—the incidence at which the pressure distribution is the same on both sides of the blade;
- $\alpha = -6.5°$—represents the value at which the helicopter maintains its stable position on the yaw axis;
- $\alpha = -15.5°$—is the maximum negative value of the incidence that the blade can achieve during flight.

The fluid flow domain defined for the CFD analysis has the shape of a rectangular parallelepiped, with the outer walls set at a distance of 1.5 m from the centrally positioned tail rotor blade. The velocity inlet section (a) and the pressure outlet section (b) are presented in Figure 17.

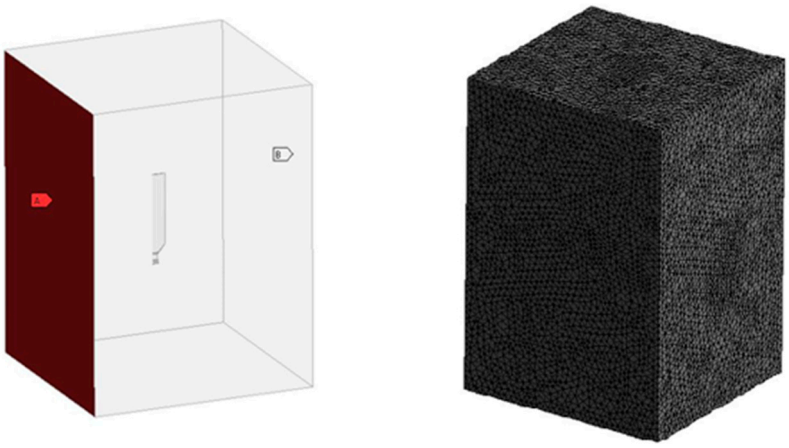

(**a**) (**b**)

**Figure 17.** Inlet and outlet sections of the fluid flow analysis: (**a**) the velocity inlet section; (**b**) the pressure outlet section.

The centre of pressure for the symmetric NACA0012 aerodynamic profile is located on the chord line at a distance of 1/4 from the leading edge and is important because the four blade incidences can be obtained by modifying the blade angle with respect to the vertical axis that runs through this point.

The fluid flow analysis was achieved with a k-ε standard fluid flow model utilized to simulate turbulent flow conditions. The fluid flow domain was set with the following property values, which are similar to sea-level conditions:

- Air pressure—101.325 kPa;
- Fluid temperature—15 °C;
- Fluid density—1.225 kg/m$^3$.

The solution was obtained after approximately 500 iterations. Figure 18 displays the pressure contour on one face of the tail rotor blade at an incidence $\alpha = 0°$. The maximum pressure region corresponds to the leading edge of the blade, with a value of 1525 Pa.

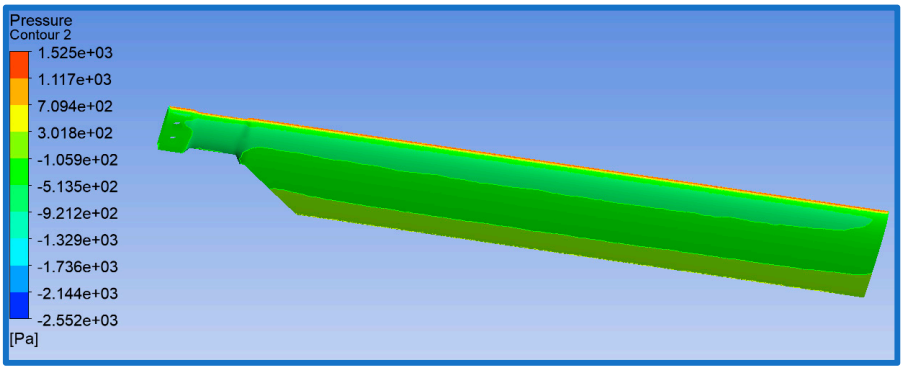


**Figure 18.** Pressure contour on one side of the tail rotor blade ($\alpha = 0°$).

Having previously determined the pressure distribution on the outer surfaces of the blade, the values were imported into a structural analysis as the loading component. All displacements were constrained on the two bolt holes positioned on the foot of the blade. The main purpose of the analysis is to analyse the mechanical response of the tail rotor blade to exterior airflow, uniformly distributed on the length of the blade. The main results for the FEA with $\alpha = 0°$ are presented in Figure 19.

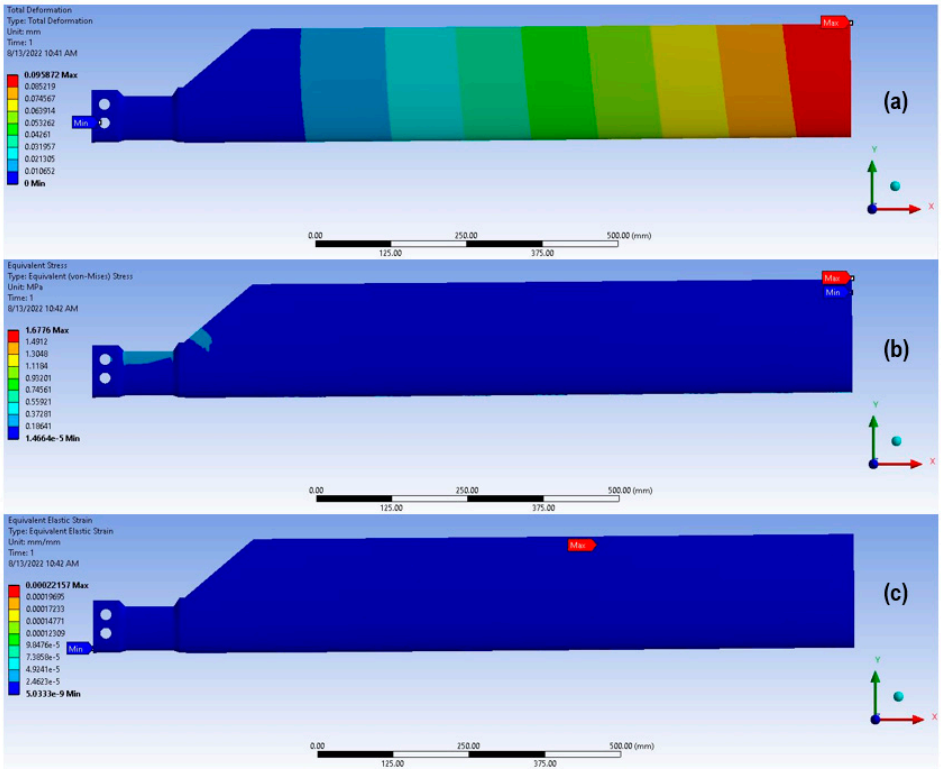


**Figure 19.** Finite element simulation results—(**a**) total displacement, (**b**) equivalent von Mises stress, (**c**) equivalent Elastic Strain.

The main results for the four studied cases are presented in Table 6. The FEA confirmed the fact that two of the tail rotor blade components are more capable of withstanding the overall stress, as opposed to the honeycomb core. The extruded honeycomb compensates, on the other hand, with a significantly lower mass and high corrosion resistance. Overall, the rigid roving spar and the composite skin compensate for the weakness of the core.

The maximum von Mises stress is located on an isolated small edge of the honeycomb core near the trailing edge. By increasing the angle of incidence, the maximum von Mises stress also has a proportional increase. The main stressed area of the spar is located at

the foot of the blade, in the direction opposed to the airflow direction, with the material being compressed in that region due to the bending of the blade. On the skin of the blade, the maximum stress values are located on the leading edge, in the area where the airflow makes direct contact with the outer surface of the skin. In the case of the honeycomb core, the maximum stress values are located on the joints of the honeycomb hexagonal cells.

**Table 6.** Main results for each incidence case.

| Blade Incidence $\alpha$ (°) | Maximum Equivalent Elastic Strain | Maximum Total Displacement (mm) | Maximum von Mises Stress (MPa) |
|---|---|---|---|
| +2.5 | 0.00022 | 0.095 | 1.68 |
| 0 | 0.00343 | 1.412 | 24.90 |
| −6 | 0.00923 | 3.807 | 66.65 |
| −15.5 | 0.02862 | 11.725 | 207.72 |

The results listed in Table 6 show the variation in the main performance indicators with respect to the blade incidence angle. It can be seen that small incidence values imply small displacement and stress output, while higher incidence values lead to significantly higher results. The blade incidence, $\alpha = -15.5°$, represents the maximum value achievable in flight by an IAR330 transport helicopter; therefore, it is a value that rarely occurs in flight and only for a limited amount of time. Thus, the higher stress value is not regarded as a factor of risk that should be taken into account.

The obtained numerical results prove that the presented research can be further continued by manufacturing a 1:1 blade and testing it directly on a helicopter.

## 7. Conclusions

The paper describes a new composite, lighter solution for the tail rotor blade of an IAR330 helicopter, with enhanced strength, durability, and maintenance properties. The novelty of the proposed blade relies on the fact that it combines hand lay-up composite material with 3D-printed composites to obtain a single aerodynamic structure, a manufacturing method not often considered for composite helicopter blades.

The numerical model of the new blade was experimentally validated by bending tests. The difference between the numerical and experimental values of the maximum bending force was 6.15%, thus showing the accuracy of the proposed model, which was further used to obtain the mechanical response of the blade loaded with aerodynamic pressures previously obtained from a fluid flow analysis. The complex numerical analyses showed the very good behaviour of the proposed composite blade during flight, with higher stresses only at the maximum incidence achieved by the helicopter during flight, which occurs very seldom and for a limited time.

One of the main advantages is that the overall cost for manufacturing the new blade at full-scale is approximately RON 2500, while the price for a new aluminium alloy tail rotor blade procured from the helicopter manufacturer is nearly four times greater due to the fact that the metal blade requires multiple manufacturing processes, working with different suppliers, and personnel with various certifications, all of which increases the total cost. Also, the hand lay-up of the composite components can be organized in a relatively small warehouse space, requiring few pieces of machinery.

**Author Contributions:** Conceptualization, A.H., Ş.-D.P.; methodology, A.-D.V., F.B. and D.V.; software, A.-D.V.; validation, A.-D.V., F.B. and D.V.; formal analysis, A.-D.V.; investigation, A.H. and F.B.; resources, D.-I.T.; data curation, D.-I.T., Ş.-D.P.; writing—original draft preparation, A.-D.V.; writing—review and editing, Ş.-D.P.; visualization, A.-D.V.; supervision, Ş.-D.P.; project administration, A.H.; funding acquisition, D.-I.T. All authors have read and agreed to the published version of this manuscript.

**Funding:** The APC was funded by the University Politehnica of Bucharest, Romania.

**Data Availability Statement:** Not applicable.

**Conflicts of Interest:** The authors declare no conflict of interest.

## References


1. Arena, M.; Chiariello, A.; Castaldo, M.; Di Palma, L. Vibration Response Aspects of a Main Landing Gear Composite Door Designed for High-Speed Rotorcraft. *Aerospace* **2021**, *8*, 52. [CrossRef]
2. Chen, Y.; Jin, L.; Tang, X.; Huang, D.; Zhang, J. Dynamic Response of a Composite Fan Blade Excited Instantaneously by Multiple MFC Actuators. *Aerospace* **2022**, *9*, 301. [CrossRef]
3. Miller, A.G.; Lovell, D.T.; Seferis, J.C. The evolution of an aerospace material: Influence of design, manufacturing and in-service performance. *Compos. Struct.* **1994**, *27*, 193–206. [CrossRef]
4. Stojkovic, M.; Butt, J. Industry 4.0 Implementation Framework for the Composite Manufacturing Industry. *J. Compos. Sci.* **2022**, *6*, 258. [CrossRef]
5. Linganiso, L.Z.; Anandjiwala, R.D. Chapter 4—Fibre-reinforced laminates in aerospace engineering. In *Advanced Composite Materials for Aerospace Engineering, Processing, Properties and Applications*; Rana, S., Fangueiro, R., Eds.; Woodhead Publishing: Cambridge, UK, 2016; pp. 101–127. [CrossRef]
6. Lee, J.Y.; Kim, K.J. Overview of Polyamide Resins and Composites: A Review. *Elastomers Compos.* **2016**, *51*, 317–341. [CrossRef]
7. Nunes, J.P.; Silva, J.F. Chapter 5—Sandwiched composites in aerospace engineering. In *Advanced Composite Materials for Aerospace Engineering, Processing, Properties and Applications*; Rana, S., Fangueiro, R., Eds.; Woodhead Publishing: Cambridge, UK, 2016; pp. 129–174. [CrossRef]
8. Giurgiutiu, V. Chapter 1—Introduction. In *Structural Health Monitoring of Aerospace Composites*; Academic Press: Cambridge, MA, USA, 2016; pp. 1–23. Available online: https://www.sciencedirect.com/book/9780124096059/structural-health-monitoring-of-aerospace-composites (accessed on 8 May 2023).
9. The American Composites Manufacturers Association (ACMA). Discover Composites. Available online: https://discovercomposites.com/transportation/commercial-aircraft/# (accessed on 9 May 2023).
10. Gardner Business Media Inc. Composites World. Available online: https://www.compositesworld.com/articles/skinning-the-f-35-fighter (accessed on 12 May 2023).
11. Global Security.org. F-22 Raptor. Available online: https://www.globalsecurity.org/military/systems/aircraft/f-22.htm (accessed on 12 May 2023).
12. Helicopter Maintenance Magazine. Carbon Fiber—A New Spin for Main and Tail Rotor Blades. Available online: https://helicoptermaintenancemagazine.com/article/carbon-fiber-%E2%80%93-new-spin-main-and-tail-rotor-blades (accessed on 12 May 2023).
13. Helicopter Maintenance Magazine. From Wood to Composite Materials the Evolution of the Rotor Blade. Available online: https://helicoptermaintenancemagazine.com/article/wood-composite-materials-evolution-rotor-blade (accessed on 12 May 2023).
14. ExpertsMind.Com. Propeller Construction, Other Engineering. Available online: http://www.expertsmind.com/questions/propeller-construction-30112157.aspx (accessed on 12 May 2023).
15. Kozaczuk, K.J. Composite technology development based on helicopter rotor blades. *Aircr. Eng. Aerosp. Technol.* **2018**, *92*, 273–284. [CrossRef]
16. Rasuo, B. Helicopter Tail Rotor Blade from Composite Materials: An Experience. *SAE Int. J. Aerosp.* **2011**, *4*, 828–838. [CrossRef]
17. Rasuo, B. Experimental Techniques for Evaluation of Fatigue Characteristics of Laminated Constructions from Composite Materials: Full-Scale Testing of the Helicopter Rotor Blades. *J. Test. Eval.* **2010**, *39*, JTE102768. [CrossRef]
18. Luczak, M.; Peeters, B.; Dziedziech, K. Static and dynamic testing of the full scale helicopter rotor blades. In Proceedings of the ISMA2010-USD2010—24th International Conference on Noise and Vibration Engineering (ISMA2010) & 3rd International Conference on Uncertainty in Structural Dynamics (USD2010), Leuven, Belgium, 20–22 September 2010; pp. 2131–2143. Available online: https://past.isma-isaac.be/downloads/isma2010/papers/isma2010_0343.pdf (accessed on 17 May 2023).
19. Kliza, R.; Scislowski, K.; Siadkowska, K.; Padyjasek, J.; Wendeker, M. Strength analysis of a prototype composite helicopter rotor blade spar. *Appl. Comput. Sci.* **2022**, *18*, 5–19. [CrossRef]
20. Sudhir Sastry, Y.B.; Bhargavi Rachana, I.; Durga Rao, K. Stress Analysis of Helicopter Composite Blade Using Finite Element Analysis. *Int. J. Eng. Res. Technol.* **2013**, *2*, 1291–1299. Available online: https://www.ijert.org/research/stress-analysis-of-helicopter-composite-blade-using-finite-element-analysis-IJERTV2IS120036.pdf (accessed on 18 May 2023).
21. Vasovic Maksimovic, I.V.; Maksimovic, K.S.; Maksimovic, M.S.; Maksimovic, S.M. Strength Analysis of Helicopter Tail Rotor Blades Made from Composite Materials. In *Experimental Research and Numerical Simulation in Applied Sciences, Proceedings of the 18th International Symposium of Organizational Sciences (SymOrg 2022), Belgrade, Serbia, 11–14 June 2022*; Mitrovic, N., Mladenovic, G., Mitrovic, A., Eds.; Springer: Berlin/Heidelberg, Germany, 2022; Volume 564, pp. 97–113. [CrossRef]
22. Filippi, M.; Zappino, E.; Carrera, E.; Castanie, B. Effective Static and Dynamic Finite Element Modeling of a Double Swept Composite Rotor Blade. *J. Am. Helicopter Soc.* **2020**, *65*, 1–12. [CrossRef]
23. Hou, W.; Zhang, W.; Wang, X.; Xing, J. Deformation analysis of composite rotor blades for a helicopter. *J. Aircr.* **2012**, *49*, 2018–2022. [CrossRef]

24. Anoshkin, A.N.; Barkanov, E.; Pisarev, P.V. Calculation and Experimental Research of the Mechanical Deformation of a Helicopter Blade Made of Composite Materials with Embedded Piezoactuators. *AIP Conf. Proc.* **2020**, *2310*, 020020. [CrossRef]
25. Balasko, M.; Svab, M.; Molnar, G.; Veres, I. Classification of defects in honeycomb composite structure of helicopter rotor blades. *Nucl. Instrum. Methods Phys. Res. A* **2005**, *542*, 45–51. [CrossRef]
26. Rayavarapu, V.K. State-of-the-Art Finite Element Modeling of Rotorcraft Main Rotor Blade for Bird Strike Damage Analysis. *J. Fail. Anal. Prev.* **2018**, *18*, 1369–1378. [CrossRef]
27. Jang, J.H.; Ahn, S.H. Numerical Analysis of Bird Strike Resistance of Helicopter Composite Rotor Blade. *J. Eng. Appl. Sci.* **2019**, *14*, 6971–6981. [CrossRef]
28. Chang, S.H.; Jung, S.N. Optimal Structural Design of Composite Helicopter Blades using a Genetic Algorithm-based Optimizer PSGA. *Compos. Res.* **2022**, *35*, 340–346. (In Korean) [CrossRef]
29. Steininger, R.; Barakos, G.N.; Woodgate, M.A. Numerical analysis of HVAB and STAR rotor blades using HMB3. In Proceedings of the AIAA SCITECH 2023 Forum, Session: Special Session: Rotor-in-Hover Simulation I, National Harbor, MD, USA, 23–27 January 2023. [CrossRef]
30. Qaderi, S.; Ebrahimi, F.; Vinyas, M. Dynamic analysis of multi-layered composite beams reinforced with graphene platelets resting on two-parameter viscoelastic foundation. *Eur. Phys. J. Plus* **2019**, *134*, 339. [CrossRef]
31. Hadăr, A.; Baciu, F.; Voicu, A.D.; Vlăsceanu, D.; Tudose, D.I.; Adetu, C. Mechanical Characteristics Evaluation of a Single Ply and Multi-Ply Carbon Fiber-Reinforced Plastic Subjected to Tensile and Bending Loads. *Polymers* **2022**, *14*, 3213. [CrossRef]
32. Baciu, F.; Hadăr, A.; Voicu, A.D.; Vlăsceanu, D.; Tudose, D.I. Experimental and Numerical Analysis of Chlorinated Polyethylene Honeycomb Mechanical Performance as Opposed to an Aluminum Alloy Design. *Materials* **2022**, *15*, 8034. [CrossRef]
33. Voicu, A.D.; Hadăr, A.; Vlăsceanu, D. Validation of a Numerical Fluid Flow Analysis for a Helicopter Tail Rotor Blade Using a Subsonic Wind Tunnel. *Macromol. Symp.* **2020**, *389*, 1900099. [CrossRef]
34. Castro Composites. Technical Data Sheet for GG285T Fabric. Available online: https://www.castrocompositesshop.com/en/index.php?controller=attachment&id_attachment=935 (accessed on 25 May 2023).
35. Derakane™ | INEOS Composites. Technical Data Sheet for the Momentum 470-300 Epoxy Resin. Available online: https://3.imimg.com/data3/IU/GR/MY-3370540/derakane-momentum-470-300.pdf (accessed on 25 May 2023).
36. Toray Carbon Fibers Europe S.A. Technical Data Sheet for T300/FT300 High Performance Carbon Fiber. Available online: https://toray-cfe.com/wp-content/uploads/2020/12/toray-torayca-t300ft300-haute-resistance.pdf (accessed on 25 May 2023).
37. Fillamentum Addi(c)tive Polymers. Technical Data Sheet for CPE CF112 Carbon. Available online: https://fillamentum.com/wp-content/uploads/2020/10/TDS_CPE-CF112-Carbon.pdf (accessed on 25 May 2023).
38. *ASTM D3039/D3039M-00*; Standard Test Method for Tensile Properties of Polymer Matrix Composite Materials. ASTM International: West Conshohocken, PA, USA, 2017. Available online: https://www.astm.org/d3039_d3039m-08.html (accessed on 11 May 2023).
39. *ASTM C365/C365M-22*; Standard Test Method for Flatwise Compressive Properties of Sandwich Cores. ASTM International: West Conshohocken, PA, USA, 2022. Available online: https://www.astm.org/c0365_c0365m-22.html (accessed on 11 May 2023).
40. Voicu, A.D. Experimental and Theoretical Study of the Transition Towards a Composite Configuration for the IAR330 Tail Rotor Blade. Ph.D. Thesis, University Politehnica of Bucharest, Bucharest, Romania, 2022. Available online: https://upb.ro/studiul-teoretic-si-experimental-privind-tranzitia-palei-anticuplu-a-elicopterului-iar330-catre-o-configuratie-constructiva-compozita-experimental-and-theoretical-study-of-the-transition-towards-a-c/ (accessed on 10 May 2023). (In Romanian)
41. Al-Khudairi, O.; Hadavinia, H.; Little, C.; Gillmore, G.; Greaves, P.; Dyer, K. Full-Scale Fatigue Testing of a Wind Turbine Blade. *Materials* **2017**, *10*, 1152. [CrossRef] [PubMed]
42. Nielsen, P.H.; Berring, P.; Pavese, C.; Branner, K. *Rotor Blade Full-Scale Fatigue Testing Technology and Research*; DTU Wind Energy: Roskilde, Denmark, 2013. Available online: https://orbit.dtu.dk/files/118186769/Rotor_blade_full_scale_fatigue.pdf (accessed on 10 May 2023).
43. Blaest. Blade Test Centre. Available online: https://blaest.com/fatigue-test/ (accessed on 26 May 2023).
44. ANSYS Inc. *ANSYS Workbench User's Guide, Release 2021 R2*; ANSYS Inc.: Canonsburg, PA, USA, 2022; Available online: https://www.ansys.com/ (accessed on 16 May 2023).